

# Mechanical properties and microstructure of austenitic stainless steel after welding and post-weld heat treatment

S. Kožuh<sup>1\*</sup>, M. Gojić<sup>1</sup>, L. Kosec<sup>2</sup>

<sup>1</sup>*Faculty of Metallurgy, University of Zagreb, Aleja narodnih heroja 3, 44103 Sisak, Croatia*

<sup>2</sup>*Faculty of Natural Sciences and Engineering, University of Ljubljana, Aškerčeva 12, 1000 Ljubljana, Slovenia*

Received 8 January 2007, received in revised form 25 February 2009, accepted 26 February 2009

## Abstract

The subject of investigation was the effect of post-weld heat treatment (PWHT) on mechanical properties, hardness distribution across the welded joints, and on the microstructure of AISI 316L austenitic stainless steel weld metal. Steel plates of 15 mm thickness were welded by manual electric arc welding and treated at 600–900 °C. The tensile strength increased and impact energy values decreased with the increasing annealing temperature. The hardness test results for the weld metal, which were approximately equal before PWHT and after it, were higher than those for the base metal and the heat-affected zone. The weld metal microstructure was examined by means of an optical microscope and a scanning electron microscope. It demonstrated the presence of austenite, ferrite and microslag inclusions before PWHT, and that of sigma phase after PWHT. Also, the presence of complex Mn-Cr-Si-Ti inclusions in small holes was observed in tensile and impact (Charpy) tested specimens.

**Key words:** austenitic stainless steel, welding, mechanical properties, microstructure, sigma phase

## 1. Introduction

Since their introduction in the early 1900's austenitic stainless steels have assumed an important role in the modern world [1]. Their continuing development has generated complex steel compositions with substantial amounts of alloying elements. Austenitic stainless steels constitute the largest stainless steel family in terms of alloy type and usage. More than half of those in use are types AISI 304 and 316, that is their low-carbon grades AISI 304L and 316L [2]. Introduction of molybdenum in AISI 316L was intended primarily to improve resistance against pitting corrosion and creep resistance at elevated temperatures. As construction materials, austenitic stainless steels have found a wide range of applications. They are used at temperatures, which range from the cryogenic, where they exhibit high toughness, to elevated temperatures, where they exhibit good oxidation resistance. Owing to their mechanical properties and excellent corrosion resistance they are often used in the food industry, in chemical, petrochemical and oil industries, in bio-

medicine, for marine purposes, i.e. wherever exposure to corrosion media is involved [1]. Besides acceptable yield strength and tensile strength austenitic stainless steels are characterized by high impact energy and relatively low hardness. When considering the operational performance of austenitic stainless steel weldments, the most important points to be taken into account are corrosion resistance, weld metal mechanical properties and the integrity of the welded joint.

Austenitic steels may undergo microstructural changes in the course of the welding process or when they are exposed to elevated temperature for a shorter or longer period of time [3]. Microstructural variations caused by welding and post-weld heat treatment (PWHT) are responsible for changes in the mechanical properties and corrosion resistance of welded joints [4, 5]. The knowledge of critical cooling rates is especially important if undesirable phase transformations are to be avoided. Three intermetallic phases most frequently encountered in austenitic stainless steels are sigma phase, chi phase and Laves phase [6–8]. For welding purposes it is therefore important

\*Corresponding author: e-mail address: [kozuh@simet.hr](mailto:kozuh@simet.hr)

Table 1. Chemical composition of the base metal (wt.%)

C	Mn	Si	Cu	V	Mo	Al	Cr	Ni	W	Ti	Co	Nb
0.026	1.49	0.45	0.35	0.060	2.04	0.008	16.75	10.80	0.066	0.081	0.20	0.016

to take into consideration the weld metal ferrite content, vermicular and lathy. At 475 °C delta ferrite will undergo transformation and segregate into ferromagnetic delta ferrite and paramagnetic delta ferrite. At higher temperatures (550–900 °C) ferrite may transform to a hard and brittle sigma phase, and reduce impact energy, ductility and corrosion resistance [6, 9]. The volume fraction of sigma phase will increase with the length of heat treatment [3, 10]. By heating at 1040–1090 °C and rapid cooling sigma phase can be removed, but the procedure is not always applicable in practice.

The precipitation mechanism has been the subject of many investigations motivated by the detrimental effects of the precipitated phases on impact energy and corrosion resistance of steels [2, 11–13]. Padilha et al. [2, 11] and Sourmail [12] reported the precipitation of carbides ( $M_{23}C_6$ , MC,  $M_6C$ ,  $M_7C_3$ ), primary nitrides (MN, M = Zr, Ti, Nb, and V), and secondary nitrides ( $M_2N$ , M = Cr, Fe) in austenitic stainless steels during thermal treatment (annealing) and welding. Carbide precipitation is a phenomenon that can reduce corrosion resistance of stainless steel. It will depend upon two factors: the temperature and the carbon content. The temperature in the range from 550 to 900 °C allows chromium to diffuse away from the grain boundaries and to form carbides. The precipitation stages in the heat treatment of 316L austenitic stainless steel were also investigated by Wasnik et al. [13].

During use of stainless steels for chemical and petrochemical facilities unexpected fractures can often appear. For this reason it is necessary to be acquainted with fractographic analysis of fracture surfaces after tensile and impact energy of welded joint. Ševc et al. [14] investigated fracture surfaces of 19Cr-13Ni austenitic stainless steel after holding at elevated temperatures. On fracture surfaces two types of facets were observed: intergranular zones with dimple morphology and transgranular cleavage zones.

The importance of microstructural investigations of weld and base metals after welding and PWHT needs to be emphasized. As most mechanical, physical and chemical properties are determined by microstructure, it is very important to characterize the microstructures obtained during production and treating of austenitic stainless steel. This work is focussed on the effect of annealing temperature on the mechanical and microstructural properties. Among the principal aims of the work were established mechanisms of occurrence of intermetallic sigma phase, and determined

how mechanical properties and impact energy of austenitic stainless steel AISI 316L weld metal were affected by precipitation of sigma phase. The objective of the study was also to find correlation between delta ferrite decomposition ratio and sigma phase formation. On the other hand, interpretation of the fracture mechanism can provide valuable evidence for the cause of failure.

## 2. Experimental

Plates of 15 mm thickness, made from AISI 316L austenitic stainless steel (Table 1) were prepared as V-joints by manual electric arc welding using Böhler FOX SAS-4A electrodes. To ensure the quality of weld the edges were thoroughly cleaned. For root welding a solid electrode 2.5 mm in diameter was used while fillet welding was carried out with a 3.25 mm electrode. Immediately after welding the welded joint was subjected to PWHT at 600–900 °C for two hours, and was then cooled in the air.

For hardness and microstructure testing samples were cut out from the base metal and the welded plate. Sections of the welded joint 25 mm in length (cross-section  $15 \times 15 \text{ mm}^2$ ) with the weld metal in the middle were cut out from the welded plate and mechanically polished. Electrolytic etching was carried out with various etchants. To expose austenite boundaries 60 ml  $\text{HNO}_3$  and 40 ml water solution at 1 V dc for 20 s was used. Sigma phase and ferrite solution were identified with 56 g KOH in 100 ml water at 2 V dc for 10 s.

Hardness was measured by the Vickers test at 30 kg load across the welded joint. For microhardness measurement the same method was applied, at 1 kg load, using a Leica VMHT device.

Impact tests were performed on Charpy V-notch specimens ( $10 \times 10 \times 55 \text{ mm}^3$ ) at room temperature. A V-notch of 2 mm depth was machined in the middle of a weld metal sample. Tensile testing was carried out at room temperature with an Instron tensile machine, type 1196, on both unwelded and welded specimens. The weld metal was positioned in the middle of the gauge measure.

The delta ferrite content of base and weld metals was measured using a ferritscope. This method takes advantage of the fact that ferrite is magnetic while austenite is not.

For microstructure examination an optical microscope and a scanning electron microscope (SEM)

Table 2. Mechanical properties of the base and weld metals before PWHT, tested at room temperature

	Yield strength (N mm <sup>-2</sup> )	Tensile strength (N mm <sup>-2</sup> )	Reduction of area (%)	Impact energy (J)
Base metal	270.7	606.3	75.1	238.3
Standard deviation	15.06	4.50	1.47	4.03
Weld metal	–	732.7	52.1	83.3
Standard deviation	–	18.83	20.22	1.70

Table 3. Mechanical properties of the weld metal after PWHT at various temperatures, tested at room temperature

Temperature of annealing (°C)	Tensile strength (N mm <sup>-2</sup> )	Reduction of area (%)	Impact energy (J)
600	819.3	41.1	69.3
Standard deviation	14.61	3.83	4.11
700	835.0	34.9	43.3
Standard deviation	18.8	2.97	6.18
800	836.0	9.1	7.3
Standard deviation	9.33	3.42	1.89
900	791.0	11.6	8.0
Standard deviation	21.77	0.06	0.82

equipped with a unit for energy dispersive X-ray (EDX) spectroscopy were used.

Fracture surface testing was carried out on samples after tensile and impact testing. The SEM and EDX methods were applied to examine the weld fracture surface and to determine the effect of microstructure on fracture.

### 3. Results and discussion

From the results of this investigation it was possible to establish a correlation between the mechanical properties of the weld metal and its microstructural features at various annealing temperatures.

Tables 2 and 3 show the results of tensile testing for base and weld metals, along with standard deviations. The values are given as means of three determinations. The tensile strength of the weld metal was higher than that of the base metal. The area reduction for the weld metal decreased with a rise in the annealing temperature. The impact energy of the weld metal remarkably decreased with the increasing annealing temperature (Fig. 1). The most likely reason for this was precipitation of sigma phase. The role of sigma phase is to improve strength and reduce plasticity and toughness.

Tables 4 and 5 present the hardness test results for base and weld metals before and after PWHT. Figure

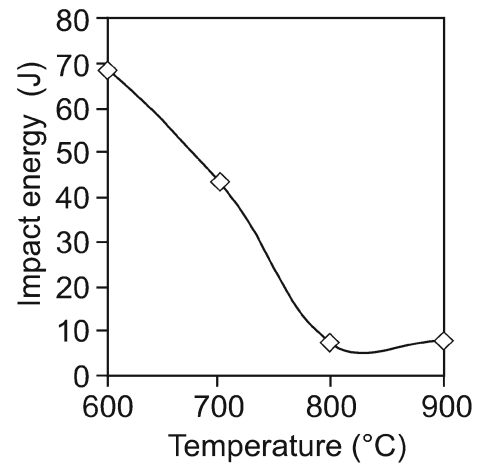


Fig. 1. Effect of annealing temperature on tensile strength (a), area reduction (b) and impact energy (c) of the weld metal.

2 shows Vickers hardness (a) and microhardness (b) distribution in the welded parts after welding and after PWHT at 800°C. The hardness values after PWHT were negligibly lower than microhardness values. The hardness values of the weld metal were higher (Fig. 3), and of the base metal lower (Table 4) than those of the HAZ. The remarkably higher hardness values for the weld metal could be accounted for its chromium con-

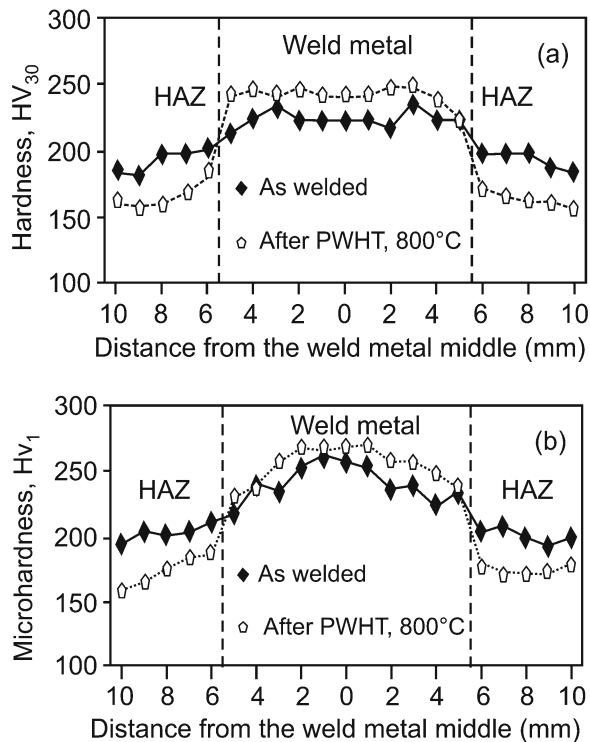


Fig. 2. Distribution of Vickers hardness  $HV_{30}$  (a) and microhardness  $HV_1$  (b) of welded parts after welding and after PWHT.

tent of about 19.0 wt.% (Table 6), which was higher than in the base metal (Table 1). The elevated chromium content in the weld metal, along with the presence of niobium, has been reported to increase steel hardenability [1]. This is in agreement with the results of Ohkubo et al. [15] who investigated the effect of alloying elements on the mechanical properties of austenitic stainless steel. Increased weld metal hardness could also be due to the heat input from welding, melting and solidification of the area.

Measurements of hardness distribution in the weld metal before PWHT and after it failed to show a significant difference. The average hardness was 224  $HV_{30}$  before PWHT, and from 232 to 241  $HV_{30}$  after annealing. After PWHT hardness values diminished for both the base metal and the HAZ. This could be at-

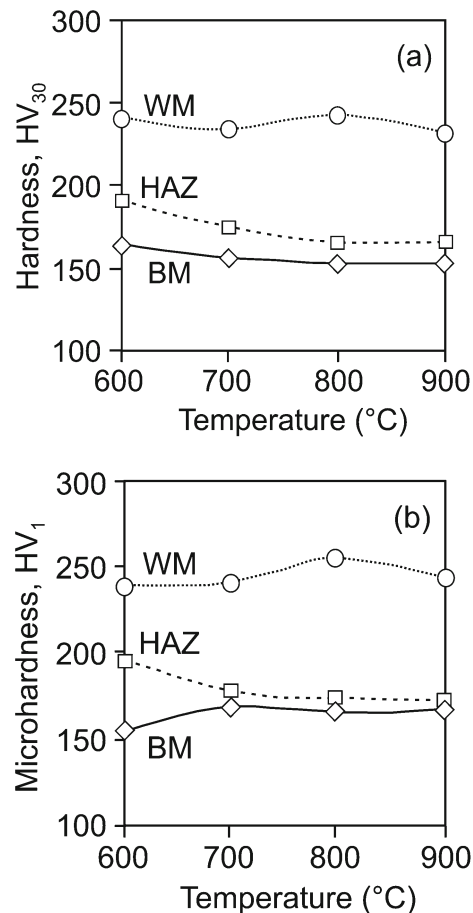


Fig. 3. Effect of annealing temperature on hardness (a) and microhardness (b) of the base metal (BM), the heat-affected zone (HAZ) and the weld metal (WM).

tributed to a lower stress level and to a change in microstructure.

The microstructure that evolves in a weldment is heterogeneous owing to the temperature gradient associated with the welding process and the chemical gradient, which is generated during that process. Once the peak temperatures have been attained, the subsequent cooling rates will decrease with the increasing distance from the fusion boundary, leading to the formation of various non-equilibrium microstructures.

Table 4. Hardness test results for the base and weld metals before PWHT

	Hardness $HV_{30}$			Microhardness $HV_1$		
	BM	HAZ	WM	BM	HAZ	WM
Base metal	167.3	–	–	154.8	–	–
Standard deviation	2.49	–	–	4.87	–	–
Weld metal	167.3	192.8	224.2	154.8	201.7	239.3
Standard deviation	2.49	7.40	6.10	4.87	4.99	13.17

Table 5. Hardness test results for the base and weld metals after PWHT

Temperature of annealing (°C)	Hardness HV <sub>30</sub>			Microhardness HV <sub>1</sub>		
	BM	HAZ	WM	BM	HAZ	WM
600	164.3	189.5	240.9	153.9	194.9	239.8
Standard deviation	0.95	5.89	8.96	2.21	9.66	10.88
700	155.6	173.6	233.7	168.0	177.6	241.0
Standard deviation	0.95	8.90	9.19	9.22	8.00	16.78
800	152.3	165.3	241.5	165.7	174.1	254.8
Standard deviation	2.06	8.52	6.50	3.07	7.52	13.58
900	153.3	166.2	232.2	167.4	172.0	244.6
Standard deviation	2.36	7.30	5.57	14.4	7.21	9.92

Table 6. Chemical composition of the weld metal (wt.%)

C	Mn	Si	Cu	V	Mo	Al	Cr	Ni	W	Ti	Co	Nb
0.024	0.85	0.74	0.11	0.074	2.44	0.004	19.15	10.86	0.048	0.009	0.095	0.289

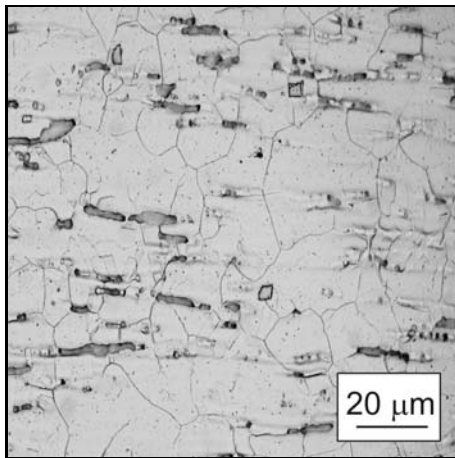


Fig. 4. Optical micrograph of AISI 316L stainless steel base metal.

As a result of microstructural inhomogeneity gradients in mechanical properties may become noticeable across the weldment.

Ideally, austenitic stainless steels will exhibit a single phase that is maintained over a wide temperature range. However, a fully austenitic microstructure is more crack sensitive than the one containing a small amount of ferrite. Figure 4 shows an austenitic polygonal grain of AISI 316L stainless steel base metal with a low delta ferrite content. Grain size was 7.58, and average grain area 679  $\mu\text{m}^2$  with 1496 grains/unit area. Stringers of delta ferrite can be seen elongated in the rolling direction. Phase transformations in austenitic stainless steels can be determined with the help of chromium and nickel equivalencies [16].

For AISI 316L austenitic stainless steel base metal used in this work, the  $\text{Cr}_{\text{eq}}/\text{Ni}_{\text{eq}}$  ratio was 1.59. The final microstructure, according to Schaeffler diagram [16], consisted of austenite and about 5 % delta ferrite. The latter corresponded to the measured delta ferrite content of 3.4 %. The amount of ferrite that formed in the base metal microstructure was sensitive to small changes in the cooling rate. It is generally held that a 4–8 % delta ferrite content in the base metal is an effective means of offsetting a grain boundary weakness that develops in austenite at high temperatures and leads to fissuring. The ferrite ability to reduce hot cracking is attributed to the prevention of segregation of low-melting constituents such as sulphur and phosphorus to the interdendritic areas. However, high ferrite has been reported to reduce corrosion resistance drastically, and to promote high-temperature embrittlement [17]. In the case of 316L stainless steel, elevated C, Mn, Ni, and N concentrations were responsible for the low ferrite number proving to be strong austenite stabilizers. The elements Cr, Si and Mo, on the other hand, are known as strong ferrite stabilizers and increase the ferrite number.

In this work the base metal microstructure differed from the microstructure of the weld metal (Fig. 5). According to [18, 19], for commercial 300-series stainless steels the weld metal solidification mode can be determined from the  $\text{Cr}_{\text{eq}}/\text{Ni}_{\text{eq}}$  ratio. In our case (Table 3)  $\text{Cr}_{\text{eq}}/\text{Ni}_{\text{eq}} = 1.91$ , solidification mode FA ( $1.48 \leq \text{Cr}_{\text{eq}}/\text{Ni}_{\text{eq}} \leq 1.95$ ). As is well known, the solidification behaviour of stainless steel weld metal can be classified into four solidification modes (A, AF, FA, and F) according to its general microstructure and delta ferrite morphology. In the case of A mode, the

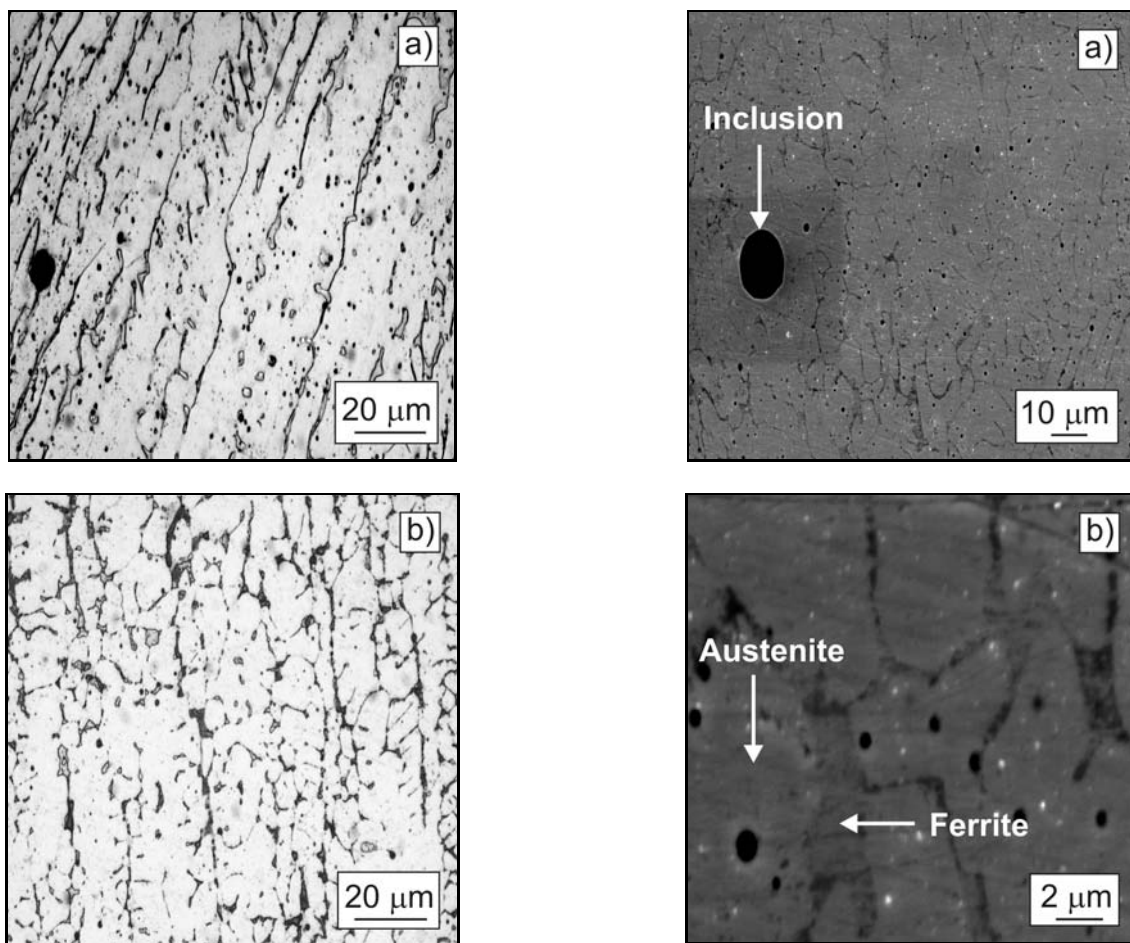


Fig. 5. Optical micrograph of AISI 316L stainless steel weld metal before PWHT (a) and after PWHT at 800°C (b).

weld metal completely solidifies to austenite. In AF mode, austenite is the leading phase and delta ferrite, if any, solidifies intergranularly from the rest melt. On the other hand, in FA mode welds delta ferrite is the leading phase and austenite solidifies from the rest melt. At lower temperature the majority of ferrite is transformed to austenite by an equiaxial or acicular mechanism, depending on the supercooling of delta ferrite. In F mode, the weld metal solidifies completely to delta ferrite, and austenite is precipitated from the solid ferrite at lower temperatures.

The delta ferrite content in the weld metal plays an important role in determining the fabrication and service performance of the welded structures. The ferrite morphology will depend on the weld section viewed. David [20] observed four distinct types of ferrite morphology in AISI 308 stainless steel with a delta ferrite content from 9 to 15 %: vermicular, lacy, acicular and globular. Variations in ferrite morphology are related to the weld metal composition, ferrite content, and ferrite distribution as a result of thermal cycling during subsequent weld passes. For selection of filler metals

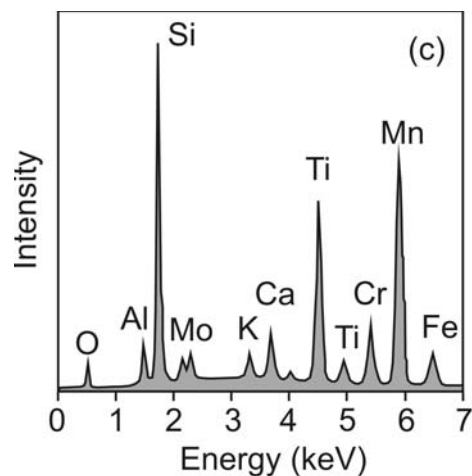


Fig. 6. SEM micrograph of AISI 316L stainless steel weld metal before PWHT: a) basic view, b) detail, c) EDX spectrum of the microslag inclusion.

estimates of the ferrite content are normally made using Schaeffler diagram. According to the diagram and the weld metal  $Cr_{eq}/Ni_{eq}$  ratio, the delta ferrite content in this work was about 16 %. Measured with a ferriscope it was 14.2 %. Elevated ferrite content in

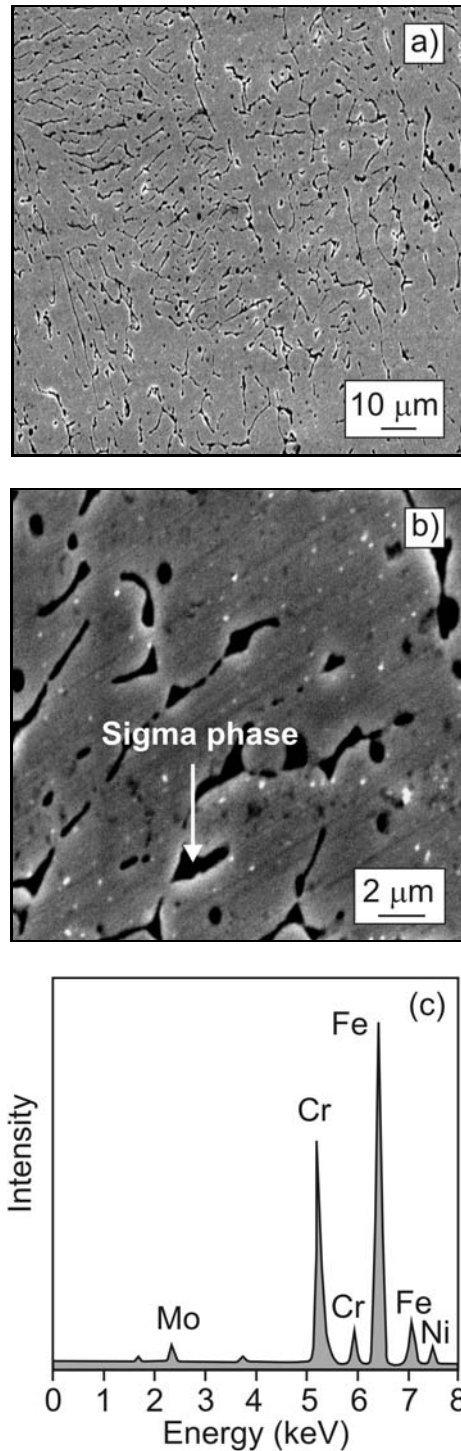


Fig. 7. SEM micrograph of AISI 316L stainless steel weld metal after PWHT at 800°C: a) basic view, b) detail, c) EDX spectrum of the sigma phase.

the weld metal poses the risk of enhancing formation of sigma phase at elevated temperature. The presence of sigma phase in the weld metal before PWHT was not observed (Fig. 6).

Figure 6 is a scanning electron micrograph of the

weld metal before PWHT. In Fig. 6a a complex microslag inclusion can be seen. During tensile testing, the impurity particles fractured or broke off. The weld metal microstructure before PWHT consists of austenite and ferrite (Fig. 6b). In the microstructure sporadically were observed complex microslag inclusions and the EDX spectrometry showed manganese, silicon, titanium and chromium to be dominant elements in the inclusions (Fig. 6c). In Table 7 the EDX results are presented in the quantitative form. The nickel content was higher in austenite because nickel acted as its stabilizer. In contrast, chromium content was higher in ferrite.

The weld metal microstructure after PWHT consisted of austenite grains with sigma phase particles (Fig. 7). Sigma phase is a well-known intermetallic phase, which forms in the Fe-Cr system between 550 and 900°C. As seen in Fig. 7a, and in more detail in Fig. 7b, sigma phase particles were observed at ferrite/austenite grain boundaries. The sigma phase morphology was usually equiaxed. The presence of sigma precipitates in microstructure can lead to degradation of corrosion resistance, localized stresses at the interfaces between sigma particles and the matrix, altered crack propagation behaviour, and reduced fracture toughness. As shown by EDX analysis, iron, chromium and nickel were dominant elements in sigma phase (Fig. 7c). In this work the sigma phase composition was 65–67 % Fe, 22–26 % Cr, 5–7 % Ni and about 1 % Mo. It was slightly different from the typical sigma phase composition of AISI 316 or 316L austenitic stainless steels (in wt.%), which is 55 % Fe, 29 % Cr, 11 % Mo and 5 % Ni [2]. In contrast, Dománková et al. [8] suggested the following sigma phase composition in AISI 316 after ageing at 800°C: 56–61 % Fe, 21–26 % Cr, 12–21 % Mo and 1–5 % Ni. As the sigma phase composition tends to vary it is difficult to define it by a formula. Sigma phase precipitation tends to deplete the adjacent matrix of chromium. The presence of the chromium-depleted zones, which are possible points for pitting, can enhance embrittlement in pitting resistance. After heat treatment the precipitation of brittle sigma phase produced a considerable drop in impact energy values (Table 3).

The mechanism of sigma phase nucleation is still a matter of controversy and depends on the amount of delta ferrite. The delta ferrite content in the weld metal decreased with the increasing annealing temperature (Table 8). Its transformation was calculated from the values measured before heat treatment and after it. The ratio of delta ferrite decomposition in the weld metal was highly dependent on increase in the annealing temperature. The delta ferrite decomposition ratios in samples annealed at 600, 700, 800, and 900°C were 17.6, 43.6, 93.7, and 96.5 %, respectively. Transformation of vermicular and lathy delta ferrite into sigma phase was a function of the chemical com-

Table 7. Results of EDX analysis of different position in weld metal before PWHT (wt.%)

Position	C	O	Al	Si	K	Ca	Ti	Cr	Mn	Fe	Mo	Ni
Inclusion	–	3.92	2.31	19.58	1.50	3.34	18.39	8.39	37.01	1.68	3.01	–
Ferrite	1.67	–	–	–	–	–	–	22.10	0.81	65.28	2.96	6.54
Austenite	1.62	–	–	–	–	–	–	17.47	0.75	66.63	1.64	11.27

Table 8. Delta ferrite content in the base and weld metals after PWHT (wt.%)

Temperature of annealing (°C)	600	700	800	900
$\delta$ -ferrite in base metal (%)	2.6	1.2	0.4	0.7
$\delta$ -ferrite in weld metal (%)	11.7	8.0	0.9	0.5

Table 9. Chemical composition of Mn-Cr-Si-Ti inclusions shown in Figs. 10 and 11 (wt.%)

Position	O	Al	Si	Mo	Ti	Cr	Mn	Fe	Ni
Inclusion 1	2.9	1.1	19.3	1.2	12.4	20.8	37.8	3.6	–
Inclusion 2	1.7	1.3	17.2	1.5	4.9	9.6	54.5	7.9	1.1

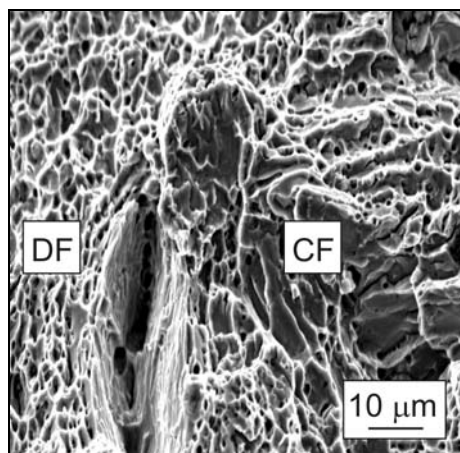


Fig. 8. SEM microfractograph of AISI 316L austenitic stainless steel weld metal after Charpy impact testing. DF – ductile fracture, CF – cleavage fracture.

position of the weld metal. Barcik [21] claimed that the kinetics of sigma phase precipitation was governed by the rate of diffusion of chromium and other sigma-forming elements. In this work the sigma precipitation rate was enhanced as the result of the PWHT temperature. Wegrzyn et al. [22] who investigated the effect of alloying elements on sigma phase formation in 18-8 weld metals reported that the weld metal containing high molybdenum was most prone to forming sigma phase from delta ferrite and that ferrite transformation to sigma phase was highest at about 750°C. Next came silicon, tungsten, vanadium, and niobium in diminishing order. Copper, on the other hand, acted by delaying delta ferrite transformation to sigma phase.

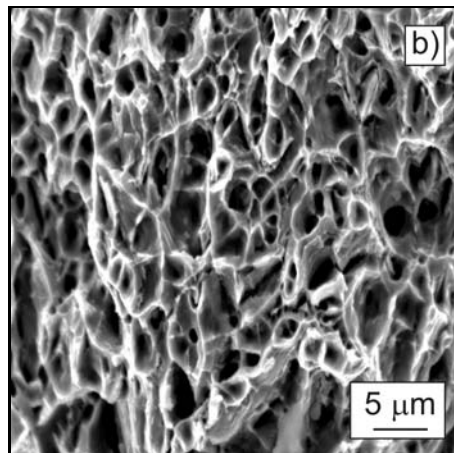
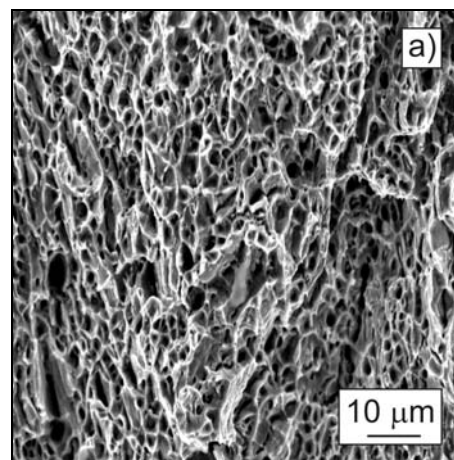


Fig. 9. SEM microfractograph of AISI 316L austenitic stainless steel weld metal after tensile testing: a) basic view, b) detail. Specimens annealed at 600°C.

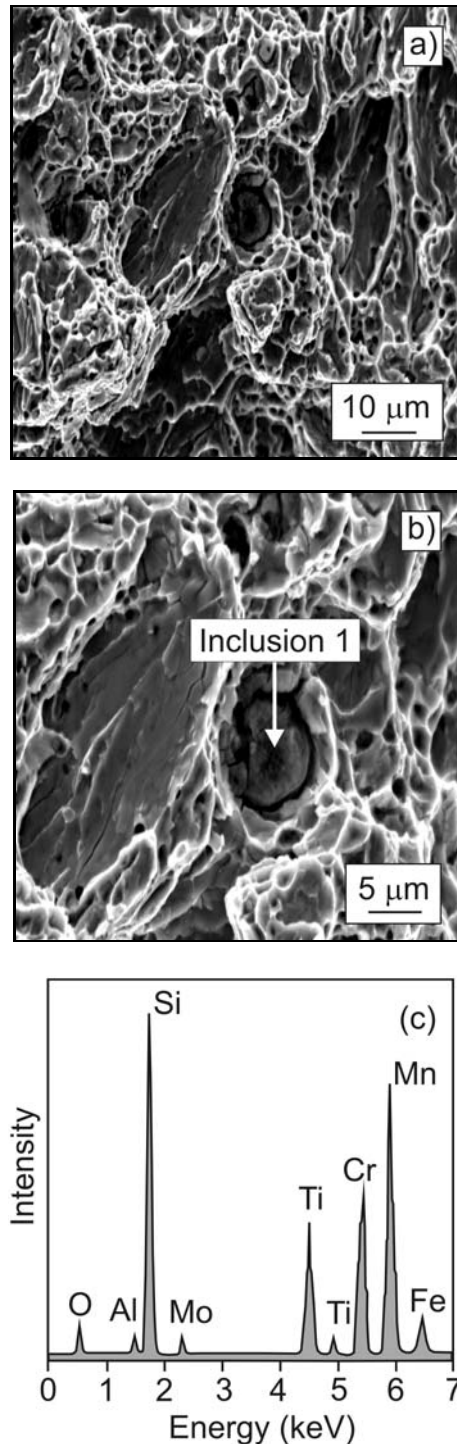


Fig. 10. SEM microfractograph of AISI 316L austenitic stainless steel weld metal after tensile testing: a) basic view, b) detail, c) EDX spectrum of complex Mn-Cr-Si-Ti inclusion. Specimens annealed at 800 °C.

According to the investigation into the kinetics of delta ferrite transformation in type 316 stainless steel weld metal by Mudali et al. [5] almost 70 % of ferrite transformation was complete at 750 °C/0.5 h, sigma

precipitation having already taken place in ferrite particles. A continuous ferrite network was broken and the secondary dendrite arms had undergone spheroidization. The kinetics of precipitation at 850 °C was very rapid and a ferrite transformation of about 90 % was observed at 0.5 h. This transformation increased with ageing. Ageing up to 100 h showed the formation of a blocky sigma phase inside delta ferrite cores. Sourmail et al. [23] observed a slower rate of sigma phase formation in AISI 316 than in AISI 347, and an increase with ageing at 700 °C.

It is well known that fractography directly describes the fracture process and provides valuable evidence for the cause of failure [14, 24]. In this work we investigated the fracture surface of austenitic stainless steel after tensile and impact testing. Two distinct fracture modes were observed, a ductile fracture (Figs. 8, left, and 9) and a cleavage fracture with a small number of dimples (Fig. 8, right). The ductile fracture was characterized by void nucleation, growth and coalescence. At the annealing temperature of 800 °C the fracture surface of the weld metal revealed primarily a cleavage fracture in both tensile and impact tested specimens (Figs. 10a,b and 11a). On the microfractograph a number of inclusions in small holes can also be observed. The EDX analysis demonstrated the presence of complex Mn-Cr-Si-Ti inclusions of different composition (Figs. 10c and 11b, Table 9).

#### 4. Conclusions

Results of investigation into the properties of high-alloyed AISI 316L austenitic stainless steel before PWHT and after it allow drawing the following conclusions:

1. The tensile strength of the weld metal was higher than that of the base metal. The area reduction for the weld metal decreased with the increasing annealing temperature. The impact energy values drastically decreased with the increasing annealing temperature.

2. The hardness and microhardness test results for the weld metal were remarkably higher than those for the base metal. The hardness values of the weld metal varied insignificantly before PWHT and after it. After PWHT they were lower for both the base metal and the HAZ.

3. The base metal consisted mainly of polygonal austenite grains and a small amount of delta ferrite. The delta ferrite content was 3.4 % as compared to 14.2 % in the weld metal. The delta ferrite content decreased with the increasing annealing temperature.

4. The ratio of the delta ferrite decomposition in the weld metal was highly dependent on increase in the annealing temperature. It was increased from 17.6 % at 600 °C to 96.5 % at 900 °C.

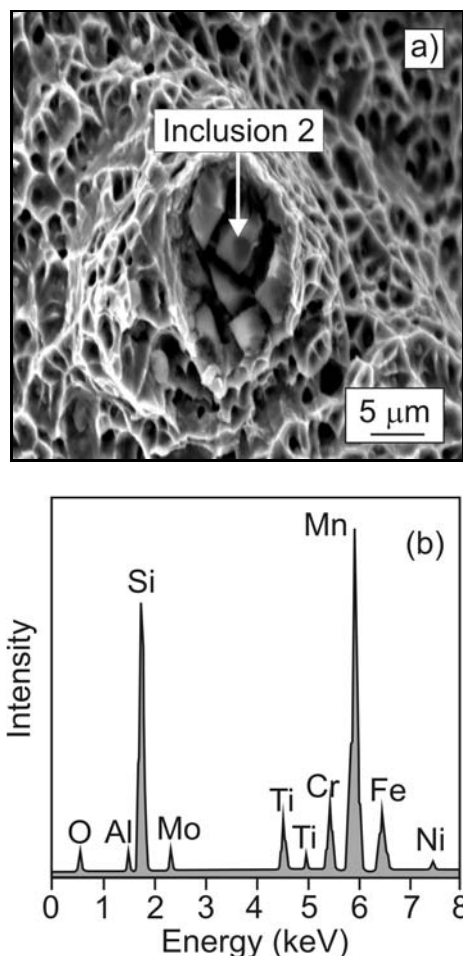


Fig. 11. SEM microfractograph of AISI 316L austenitic stainless steel weld metal after Charpy impact testing (a) and EDX spectrum of complex Mn-Cr-Si-Ti inclusion (b). Specimens annealed at 800°C.

5. Before PWHT the weld metal microstructure consisted of austenite and ferrite. Also, in the microstructure sporadically were observed complex microslag inclusions. The EDX analysis showed manganese, silicon, titanium and chromium to be dominant elements in the inclusions.

6. EDX analysis of the weld metal after PWHT showed the presence of sigma phase at ferrite/austenite grain boundaries as a result of delta ferrite transformation at elevated temperature. The sigma phase composition was 65–67 % Fe, 22–26 % Cr, 5–7 % Ni and about 1 % Mo. This was considered to be adverse to impact energy.

7. Two distinct fracture modes were observed, ductile fracture and cleavage fracture. The EDX analysis demonstrated the presence of complex Mn-Cr-Si-Ti inclusions in both tensile and impact tested specimens.

## References

- [1] LULA, R. A.: *Stainless Steel*. Metals Park, Ohio, American Society for Metals 1986.
- [2] PADILHA, A. F.—RIOS, P. R.: *ISIJ Int.*, **42**, 2002, p. 325.
- [3] MINAMI, Y.—KIMURA, H.—IHARA, Y.: *Mat. Sci. Tech.*, **2**, 1986, p. 795.
- [4] SIREESHA, M.—ALBERT, S. K.—SUNDARESAN, S.: *Mat. Sci. Tech.*, **19**, 2003, p. 1411.
- [5] MUDALI, U. K.—DAYAL, R. K.: *Mat. Sci. Tech.*, **16**, 2000, p. 393.
- [6] SONG, Y.—MCPHERSON, N. A.—BAKER, T. N.: *ISIJ Int.*, **36**, 1996, p. 1392.
- [7] HRIVŇÁK, I.: *Acta Metall. Slovaca*, **10**, 2004, p. 91.
- [8] DOMÁNKOVÁ, M.—MAGULA, V.: *Acta Metall. Slovaca*, **10**, 2004, p. 234.
- [9] ÅSTRÖM, H.: In: *Proceedings of International Conference Joining of Corrosion Resistant Materials*. Ed.: Kralj, S. Opatija, Croatian Welding Society 2003, p. 195.
- [10] KÄLLQVIST, J.—ANDRÉN, H. O.: *Mat. Sci. Eng., A270*, 1999, p. 27.
- [11] PADILHA, A. F.—PLAUT, R. L.—RIOS, P. R.: *ISIJ Int.*, **43**, 2003, p. 135.
- [12] SOURMAIL, T.: *Mat. Sci. Tech.*, **17**, 2001, p. 1.
- [13] WASNIK, D. N.—DEY, G. K.—KAIN, V.—SAMAJDAR, I.: *Scripta Materialia*, **49**, 2003, p. 135.
- [14] ŠEVC, P.—MANDRINO, D.—BLACH, J.—JENKO, M.—JANOVEC, J.: *Kovove Mater.*, **40**, 2002, p. 35.
- [15] OHKUBO, N.—MIYAKUSU, K.—UEMATSU, Y.—KIMURA, H.: *ISIJ Int.*, **34**, 1994, p. 764.
- [16] GOJIĆ, M.: *Techniques of Joining and Cutting of Materials*. Sisak, Faculty of Metallurgy, University of Zagreb, 2003 (in Croatian).
- [17] FARID, M.—MOLIAN, P. A.: *J. Mat. Sci.*, **35**, 2000, p. 3817.
- [18] WOO, I.—KIKUCHI, Y.: *ISIJ Int.*, **42**, 2002, p. 1334.
- [19] BOOTHBY, R. M.: *Mat. Sci. Tech.*, **2**, 1986, p. 78.
- [20] DAVID, S. A.: *Weld. J.*, **60**, 1981, p. 63.
- [21] BARCIK, J.: *Metall. Trans.*, **14A**, 1983, p. 635.
- [22] WEGRZYN, J.—KIMPEL, A.: *Weld. J.*, **60**, 1981, p. 146.
- [23] SOURMAIL, T.—BHADESHIA, H. K. D. H.: *Computer Coupling of Phase Diagrams and Thermochemistry*, **27**, 2003, p. 169.
- [24] CUI, Y.—LUNDIN, C. D.—HARIHARAN, V.: *J. Mat. Process. Tech.*, **171**, 2006, p. 150.